RESEARCH ARTICLE

VPS13A Deficiency Leads to Impaired Lipid Distribution and Alteration of Mitochondrial Calcium Homeostasis in Fibroblasts of VPS13A Disease Patients

Dajana Grossmann, PhD,[1] Adrian Spranger,[1] Emily Fischer,[1] Johanna W. Schubarth, MSc,[2] Jenny Leopold, PhD,[2] Hannes Glaß, PhD,[1] Sebastian Klicker, MSc,[1] My Uyen Dang Thi,[1] Anna Elisabeth Bartalis, MSc,[1] Andreas Hermann, MD, PhD,[1,3,4,5*] and Kevin Peikert, MD[1,3,5]

ABSTRACT: Background: Membrane contact sites are crucial for the exchange of ions or lipids and thus are critical for the function and maintenance of organelles. VPS13A is a membrane-residing, bridge-like protein connecting two membranes to enable bulk lipid transfer. Loss-of-function mutations in the *VPS13A* gene cause VPS13A disease. Previous studies showed alterations of lipid transfer and impaired calcium homeostasis.

Objective: Although membrane contact sites are becoming increasingly important in neurodegenerative disease research, their contribution to cellular homeostasis is still unclear. We attempted to investigate the consequences of loss of VPS13A function on membrane contact sites and related mechanisms in the context of VPS13A disease.

Methods: VPS13A-deficient patient-derived fibroblasts were compared with fibroblasts from healthy donors. Specific dyes, labeled fatty acids, and a specific marker for mitochondrial–endoplasmic reticulum contact sites were used to investigate lipid transfer and distribution in involved organelles. Mitochondrial calcium handling was investigated using the calcium indicator Rhod-2, AM. Images were obtained by super-resolution microscopy using Airyscan2 technology.

Results: We observed a general disturbance of membrane contact sites in VPS13A disease, accompanied by a reduction in lipid droplet formation, diminished lipid transfer into mitochondria, and unusual mitochondrial calcium uptake behavior in VPS13A disease fibroblasts.

Conclusions: Loss of VPS13A causes alterations beyond an impairment of lipid shuttling, which includes a dysregulation of membrane contact sites as well as impaired mitochondrial calcium handling. Accordingly, our findings contribute significantly to the understanding of mechanisms directly or indirectly linked to the function of VPS13A. © 2026 The Author(s). *Movement Disorders* published by Wiley Periodicals LLC on behalf of International Parkinson and Movement Disorder Society.

Key Words: Bridge-like lipid-transport proteins (BLTPs); calcium; lipids; MERCS; mitochondria; VPS13A

[1]Translational Neurodegeneration Section "Albrecht Kossel", Department of Neurology, University Medical Center Rostock, University of Rostock, Rostock, Germany; [2]Institute for Medical Physics and Biophysics, Medical Faculty, Leipzig University, Leipzig, Germany; [3]Center for Transdisciplinary Neurosciences Rostock (CTNR), University Medical Center Rostock, University of Rostock, Rostock, Germany; [4]German Center for Neurodegenerative Diseases (DZNE) Rostock/Greifswald, Rostock, Germany; [5]United Neuroscience Campus Lund-Rostock (UNC), Rostock, Germany

***Correspondence to:** Prof. Dr. Andreas Hermann, Translational Neurodegeneration Section "Albrecht Kossel", Department of Neurology, University Medical Center Rostock, Gehlsheimer Straße 20, 18147 Rostock, Germany; E-mail: andreas.hermann@med.uni-rostock.de

Andreas Hermann and Kevin Peikert share last authorship.

Funding agency: D.G. received funds from the German Research Foundation (DFG: GR 6326/2–1) and from the German Society for Parkinson's and Movement Disorders (Deutsche Gesellschaft für Parkinson und Bewegungsstörungen [DGP]). A.H. is supported by the Hermann und Lilly Schilling-Stiftung für medizinische Forschung im Stifterverband. K.P. was supported by Rostock Academy of Science (RAS) and the DPG. J.W.S. and J.L. were supported by the German Research Council (DFG: SCHI 476/26–1).

Received: 27 October 2025; **Revised:** 1 December 2025; **Accepted:** 17 December 2025

Published online 19 January 2026 in Wiley Online Library (wileyonlinelibrary.com). DOI: 10.1002/mds.70177

VPS13A disease, formerly known as chorea-acanthocytosis, is an ultra-rare condition caused by autosomal-recessive mutations in the *VPS13A* gene, typically causing loss of the protein.[1,2] VPS13A disease is a neurodegenerative disorder resulting in reduced quality of life and life expectancy,[1,2] characterized by morphologically altered red blood cells, so called acanthocytes, and neurological manifestations, including epileptic seizures, cognitive and behavioral impairment, and movement disorders such as chorea, dystonia, or parkinsonism arising from the degeneration of the basal ganglia.[1,3,4]

VPS13A is involved in many cellular processes like autophagy, calcium homeostasis, and the function of mitochondria and the endoplasmic reticulum (ER).[5-10] Nevertheless, only recently was VPS13A identified as a member of the bridge-like lipid transfer protein (BLTP) family.[11,12] BLTPs reside at membrane contact sites (MCS) between organelles where they facilitate lipid transfer in a non-vesicular manner.[12] VPS13A is specifically localized at MCS between the ER and mitochondria, ER and lipid droplets, ER and endosomes, or ER and the plasma membrane.[12–15]

Mitochondria–ER contact sites (MERCS) orchestrate cellular calcium homeostasis, lipid transfer, and mitochondrial function,[16-18] mechanisms that are commonly impaired in neurodegeneration.[19-21] Depending on their function, MERCS consist of different protein complexes which, contingent on the proteins involved, form different types of MERCS with variable distances between the ER and mitochondrial membranes. Wide appositions function as a hub for mitochondrial quality control[22] or may facilitate phospholipid transfer (eg, for autophagosome formation).[23,24] In contrast, narrow MERCS have been ascribed a role in the regulation of calcium homeostasis.[23,25]

Based on current knowledge of VPS13A function, we hypothesized that loss of VPS13A not only affects lipid transfer and distribution, but also directly or indirectly affects different MCS, thus further disturbing lipid and calcium homeostasis. Therefore, we aimed to study MCS, lipid transfer, and calcium exchange at MERCS for the first time in VPS13A-deficient patient-derived fibroblasts.

Materials and Methods

Cell Culture

Primary fibroblasts of unrelated controls and VPS13A disease patients (Table 1) were cultivated in Dulbecco's Modified Eagle Medium (DMEM) (+ 1% penicillin/streptomycin, + 10% fetal bovine serum; GIBCO by Thermo Fisher Scientific: 31966-021). Mycoplasma Test Kit (Promo Cell: PK-CA91-1096) was used to test for mycoplasma.

The use of patient-derived fibroblasts was in accordance with the Declaration of Helsinki (World Medical Association, 1964) and approved by the Ethical Committee of the Technische Universität Dresden (EK 393122012 and EK 45022009) and the Universität Rostock (A2019-0134), Germany. A declaration of consent was received from all participants, including for the publication of any research results.

Immunostainings and LipidTOX Staining

Fibroblasts were fixed in 4% paraformaldehyde (Morphisto: 11762.02500), permeabilized in 0.2% TritonX-100 (Roth: 3051.3; in phosphate-buffered saline [PBS]), blocked in Pierce™ protein-free blocking buffer (Thermo Fisher Scientific: 37572), then incubated with primary antibodies against TOM20 (Santa Cruz: sc-17764; 1:1000), PMP70 (Invitrogen: PA1-650; 1:1000), Catalase (Cell Signaling Technology: 12980S; 1:1000), or KDEL (Invitrogen: MA5-34715; 1:1000) and secondary antibodies Alexa Fluor-488 goat anti-mouse-IgG (Invitrogen: A11029; 1:1000) and Alexa Fluor-647 goat anti-rabbit-IgG (Invitrogen: A21245; 1:1000). Samples were stained with LipidTOX red (Invitrogen, Thermo Fisher Scientific: H34476; 1:200) and mounted in DAPI Fluoromount-G (Southern Biotechnology: 0100–20). Colocalization of different signals was assessed based on the signal overlap area of individual antibody signals, normalized per nuclei, using Fiji v1.53t.[26]

Transfections

Fibroblasts were transfected with 1 µg pDNA (either SPLICS-Mt-ER-short (Addgene: 164108), SPLICS-Mt-ER-long (Addgene: 164107), or pmRFP-LC3 (Addgene: 21075) using FuseIT DNA (Beniag: 60601). Experiments were conducted 24 hours post-transfection.

Live Cell Imaging of Lipid Droplets and Lipid Droplet Formation

Fibroblasts were stained with 100 nM MitoTracker Deep Red FM (Cell Signaling Technology: 8778) and 1 µM Bodipy493/503 (Invitrogen, Thermo Fisher Scientific: D3922) for 30 minutes at 37°C. Images were acquired at baseline and after 1 hour and 2 hours of 500 mM oleic acid (Sigma-Aldrich: 03008) application.

Live Cell Imaging of BodipyC12 Lipid Shuttling into Mitochondria

Fibroblasts transfected with SPLICS constructs (Addgene: 164108 or 164107) were incubated with 1 µM BodipyC12 (Invitrogen, Thermo Fisher Scientific: D3835) for 16 hours, followed by three times rinsing in medium and a washout phase of 1 hour. Cells were stained with 100 nM MitoTracker Deep Red FM for 30 minutes. For starvation, fibroblasts were rinsed three times in Hanks' Balanced Salt Solution (HBSS) (GIBCO

TABLE 1 *Overview of fibroblast lines*

Cell line	Sex	Clinical feature	VPS13A Western blot	Age at biopsy (years)	Mutation in the *VPS13A* gene
C_1	M	Healthy	Present	34	–
C_2	M	Healthy	Present	34	–
C_3	F	Healthy	Present	48	–
D_1	F	Parkinsonism, dystonia, epilepsy, peripheral neuropathy	Absent	46	c.4115-2923_4957-185inv (homozygous)
D_2	M	Chorea, epilepsy, peripheral neuropathy	Absent	28	c.6059delC, c.4115-2923_4957-185inv (compound heterozygous)

Abbreviations: M, male; F, female.

by Thermo Fisher Scientific: 14170088) and then incubated in HBSS for 1 or 2 hours.

Thin Layer Chromatography

For detailed method description see Supplementary Material.

Live Cell Imaging of 18:1 NBD-PS Lipid Shuttling into Mitochondria

18:1 NBD-phosphatidylserine (PS; Avanti: 810198C-1M) and 18:1 1,2-di-(9Z-octadecenoyl)-*sn*-glycero-3-phosphocholine (DOPC; Avanti: 850375C-25 mg) were mixed in a proportion of 80:20. The lipids were resuspended in Dulbecco's Phosphate-Buffered Saline (DPBS) (PAN Biotech: P04-36500). Fibroblasts were loaded with 0.2 mM 18:1 NBD-PS/DOPC and 100 nM MitoTracker Deep Red FM for 30 minutes at 37°C, then washed in DMEM+/+ and imaged at baseline conditions. For starvation conditions, fibroblasts were rinsed three times in HBSS and imaged after 1 or 2 hours in HBSS.

Live Cell Imaging of Autophagosome Formation

Fibroblasts transfected with pmRFP-LC3 (Addgene: 21075) were stained with 100 nM MitoTracker Deep Red FM, 0.2 mM 18:1 NBD-PS/DOPC, and 1 μM Hoechst for 30 minutes at 37°C. Then, fibroblasts were washed once in DMEM+/+ and imaged. Finally, the cells were rinsed three times in HBSS and imaged after 2 hours in HBSS.

Live Cell Imaging of Mitochondrial Calcium Uptake

Fibroblasts transfected with SPLICS-short were stained with 100 nM MitoTracker Deep Red FM and 1 μM Rhod-2, AM (Thermo Fisher Scientific: R1244) for 30 minutes at 37°C. Live cell microscopy was performed for 2 minutes at an interval of 10 seconds under baseline conditions. Cells were then treated with dimethyl sulfoxide (DMSO), 1 μM thapsigargin (Sigma-Aldrich: T9033-5MG), or a mixture of 1 μM thapsigargin and 10 μM Ru360 (Sigma-Aldrich: 557440-500UG) and imaging was continued for 2 minutes.

Microscopy

For microscopy, 5000 fibroblasts per well were grown in eight well high μ-Slides (Ibidi: 80806–90). All microscope imaging was performed on an inverted AxioObserver.Z1 LSM900 microscope with a super-resolution Airyscan 2 module, using a 63× 1.4 NA plan apochromat objective (Zeiss). For live cell imaging, the microscope was equipped with a Pecon incubation system to maintain 5% CO_2 and 37°C. All microscopy data were analyzed using Fiji v1.53t.[26]

Western Blot for VPS13A

Fibroblasts were lysed in radioimmunoprecipitation assay (RIPA) buffer (50 mM Tris-HCl, pH 7,4; 150 mM CaCl; 1% Triton X-100; 0.5% Na-deoxycholate; 0.1% sodium dodecyl sulfate [SDS]; cOmplete, EDTA-free protease inhibitor cocktail [Roche: 04693132001]) for 30 minutes on ice. Lysates were mixed with 5× urea buffer (200 mM glycin, 25 mM Tris-HCl, 4 M urea, 10% SDS, 400 mM DTT, 0.02% bromophenol blue; pH 6.8). SDS-PAGE (polyacrylamide gel electrophoresis) was performed using a 3%–8% Criterion XT Tris-Acetate Protein Gel (Bio-Rad: 3450129). Blotting was performed using the Trans-Blot Turbo RTA Midi 0.2 μm Nitrocellulose Transfer Kit (Bio-Rad: 1704271). Membranes were blocked in 5% milk (Carl Roth: T145.3; in TBS), then incubated with antibodies against VPS13A (Invitrogen: PA-54483; 1:500 in 5% skim milk) and β-actin (Sigma: A5441; 1:10000 in 5% skim milk) and with secondary antibodies donkey anti-rabbit-HRP (Invitrogen: A16035; 1:5000 in TBS-T) and donkey anti-mouse-HRP (Invitrogen: AA16017; 1:5000 in TBS-T). The signal was revealed using Cytiva Amersham ECL

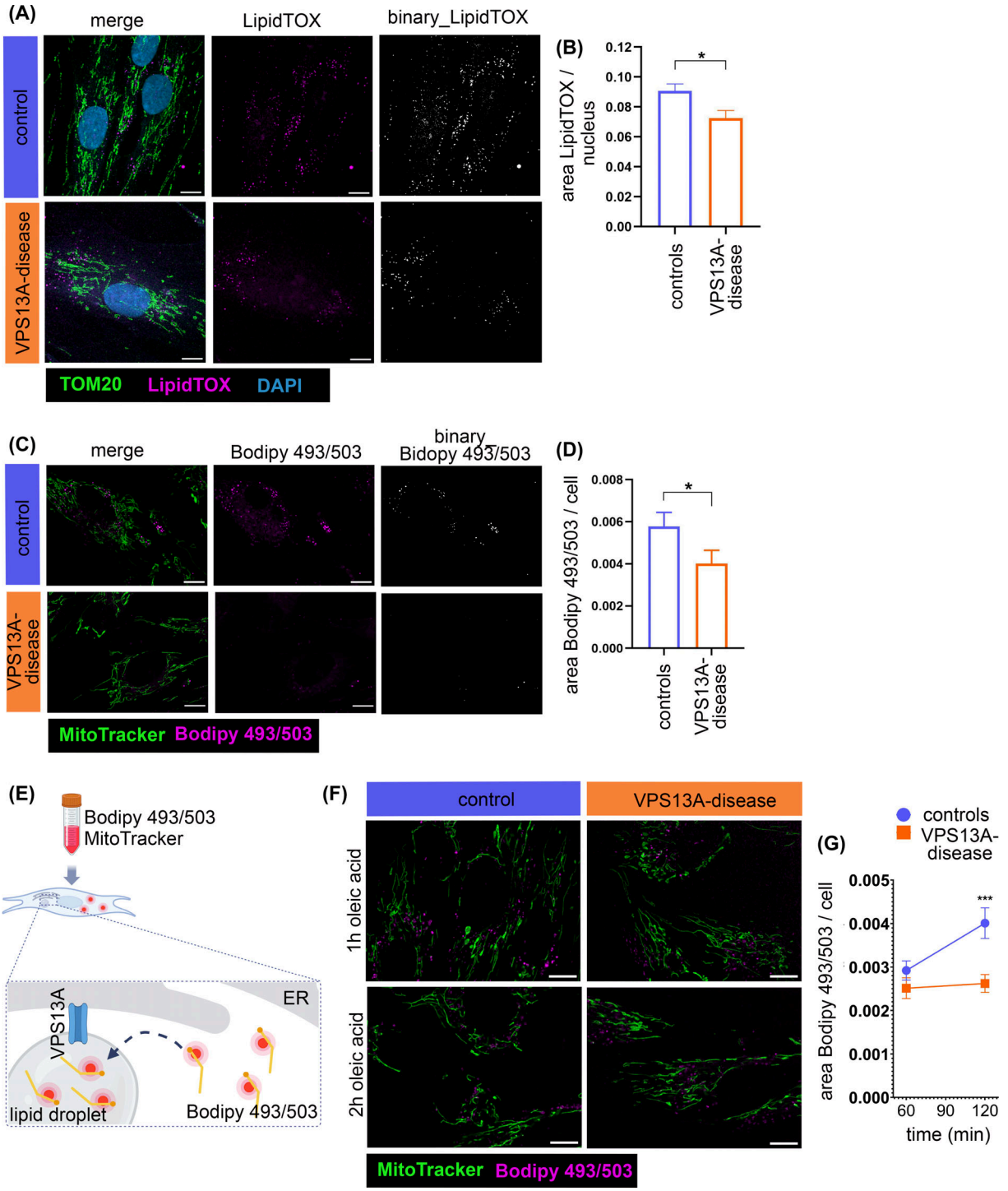

FIG. 1. Impaired lipid droplet formation in VPS13A-deficient fibroblasts. (A) Fixed fibroblasts were immunolabeled with an antibody against TOM20 (green). Lipid droplets were stained with LipidTOX (magenta). The nucleus was stained with DAPI (blue). (B) Quantification of LipidTOX area outside of the TOM20 signal, indicative for lipid droplets, normalized per nucleus. Statistical significance calculated by Mann–Whitney test (controls: $N = 14$; VPS13A disease: $N = 9$). (C) Fibroblasts were stained with MitoTracker Green FM (green) and Bodipy493/503 (magenta). (D) Quantification of the Bodipy493/503 signal area outside the MitoTracker signal, indicating lipid droplets, normalized per cell. Statistical significance calculated by Mann–Whitney test (controls: $N = 10$; VPS13A disease: $N = 3$). (E) Schematic illustration of lipid droplet formation assay using MitoTracker Deep Red FM and Bodipy493/503: Fibroblasts were stained with Bodipy493/503 and MitoTracker Deep Red FM. The Bodipy493/503 was taken up into the cytosol. Oleic acid treatment drives Bodipy493/503 incorporation into newly formed lipid droplets. Image created with Biorender.com. (F) Fibroblasts were stained with MitoTracker Deep Red FM (green) and Bodipy493/503 (magenta) and loaded with oleic acid. Images were acquired after 1 hour and 2 hours. (G) Quantification of the Bodipy493/503 signal after 1 hour and 2 hours of oleic acid incubation, normalized per cell. Statistical significance calculated by two-way analysis of variance (ANOVA) with Sidak's multiple comparison test (controls: $N = 8$; VPS13A disease: $N = 6$). Scale bars indicate 10 µm. All data are mean ± standard error of the mean (SEM). $^{*}P \leq 0.05$, $^{***}P \leq 0.001$. [Color figure can be viewed at wileyonlinelibrary.com]

Prime (Fisher Scientific/Life Science Cytiva: 10308449 [RPN2232]) on the Li-COR Odyssey XF.

Western Blot for LC3B-I/II or Mitochondrial Calcium Uniporter (MCU)

Fibroblasts were lysed in RIPA buffer. SDS-PAGE was performed using 12% self-casted polyacrylamide gels. For protein blotting, the Trans-Blot Turbo TRA Transfer Kit (Biorad: 1704271) was used. Total protein was stained with Revert 700 Total Protein Stain (LICORbio: 926-11011). Membranes were blocked in 5% milk (Carl Roth: T145.3; in TBS), then incubated with antibodies against LC3B (Cell Signaling Technology: 83506S; 1:1000 in 5% skim milk) or MCU (Proteintech: 26312-1-AP; 1:2000 in 5% skim milk) and with secondary antibodies donkey anti-rabbit-HRP (Invitrogen: A16035; 1:5000 in TBS-T) or donkey anti-mouse-HRP (Invitrogen: AA16017; 1:5000 in TBS-T). The signal was revealed using Cytiva Amersham ECL Prime.

Statistics

GraphPad Prism version 6.07 was used for statistical analyses. Data were first tested for normal distribution by a D'Agostino–Pearson omnibus normality test. Statistical tests were used as indicated in the respective figure legends. All experiments were independently repeated at least three times, defined by separate passages. For analysis, we pooled data from the control fibroblasts from three independent healthy donors and fibroblasts from two VPS13A disease patients. Results of individual lines are depicted in the Supplemental Material.

Results

Impaired Lipid Droplet Formation in Patient-Derived Fibroblasts

Primary fibroblasts of three unrelated healthy controls and two unrelated VPS13A disease patients were used (for details see Table 1). Patient-derived fibroblasts showed absence of VPS13A protein in Western blot analysis (Fig. S1). VPS13A is crucial for lipid droplet formation, but to date has only been reported in non-patient derived cells.[27,28] We used LipidTOX, which stains neutral lipids and is widely used to visualize lipid droplets.[27,28] VPS13A-deficient fibroblasts showed significantly fewer lipid droplets (Figs. 1A,B and S2A). This observation was further verified by quantification of Bodipy493/503, which also stains neutral lipids (Figs. 1C,D and S2B[28]). We next analyzed lipid droplet formation. For this purpose, fibroblasts were incubated with Bodipy493/503 and lipid droplet formation was forced with the mono-unsaturated fatty acid, oleic acid (Fig. 1E[28]). Oleic acid-induced lipid droplet formation was significantly reduced in VPS13A-deficient fibroblasts (Figs. 1F,G and S2C). Our findings demonstrate reduced formation of lipid droplets in fibroblasts from patients with VPS13A disease.

Alterations of MCS in VPS13A-Deficient Fibroblasts

Since the synthesis of various lipids requires the transfer of lipids between the ER, mitochondria, and peroxisomes, mediated in part by VPS13A, we wanted to investigate the possible phenotypes of these organelles. To this end, we immunolabeled fibroblasts with antibodies against the mitochondrial marker TOM20 and the peroxisome protein PMP70 (Fig. 2A), as peroxisomes together with mitochondria play a central role in lipid metabolism.[29,30] The ER, a crucial organelle for the synthesis of neutral lipids,[31] was visualized using an antibody against KDEL (Fig. 2B). Neutral lipids were stained with LipidTOX. While the overall area of TOM20 signal was not different between fibroblast lines (Figs. 2C and S3A), analysis of the PMP70 signal revealed increased peroxisome area (Figs. 2D and S3B). Of note, peroxisomes appear more elongated in VPS13A-deficient fibroblasts, as indicated by an increased aspect ratio (Figs. 2A,E and S3C). Additionally, we used catalase as another peroxisome marker, demonstrating a slight, yet not significant, increase in peroxisome aspect ratio (Fig. S3F–H). However, the circularity of catalase-labeled peroxisomes was reduced, pointing to alterations in shape (Fig. S3I,J). Quantification of the KDEL signal area showed no differences (Figs. 2F and S3M). The analysis of overlapping areas of different organelle markers from immunostaining uncovered increased interaction of mitochondria and peroxisomes, indicated by signal overlap of TOM20 and PMP70 (Figs. 2 and S3N), while the interaction of mitochondria (Figs. 2H and S3O) or peroxisomes with lipid droplets (Figs. 2I and S3P) was significantly reduced in VPS13A-deficient fibroblasts. The overlapping area of TOM20 and KDEL immunostaining was not changed (Figs. 2J and S3Q), while the overlapping area of KDEL with LipidTOX was reduced in VPS13A-deficient fibroblasts (Figs. 2K and S3R). These results may point to alterations in specific MCS in VPS13A-deficiency, whereas the reduction in organelle interaction with lipid droplets is likely caused by overall reduction in lipid droplets (Fig. 2).

Impaired Fatty Acid Shuttling in VPS13A-Deficient Fibroblasts

Certain lipids are formed from collaboration between the ER and mitochondria at MERCS, requiring lipid transfer by VPS13A and other lipid transfer proteins. The investigation of lipid transfer at MERCS was achieved by transfecting fibroblasts with a split-GFP

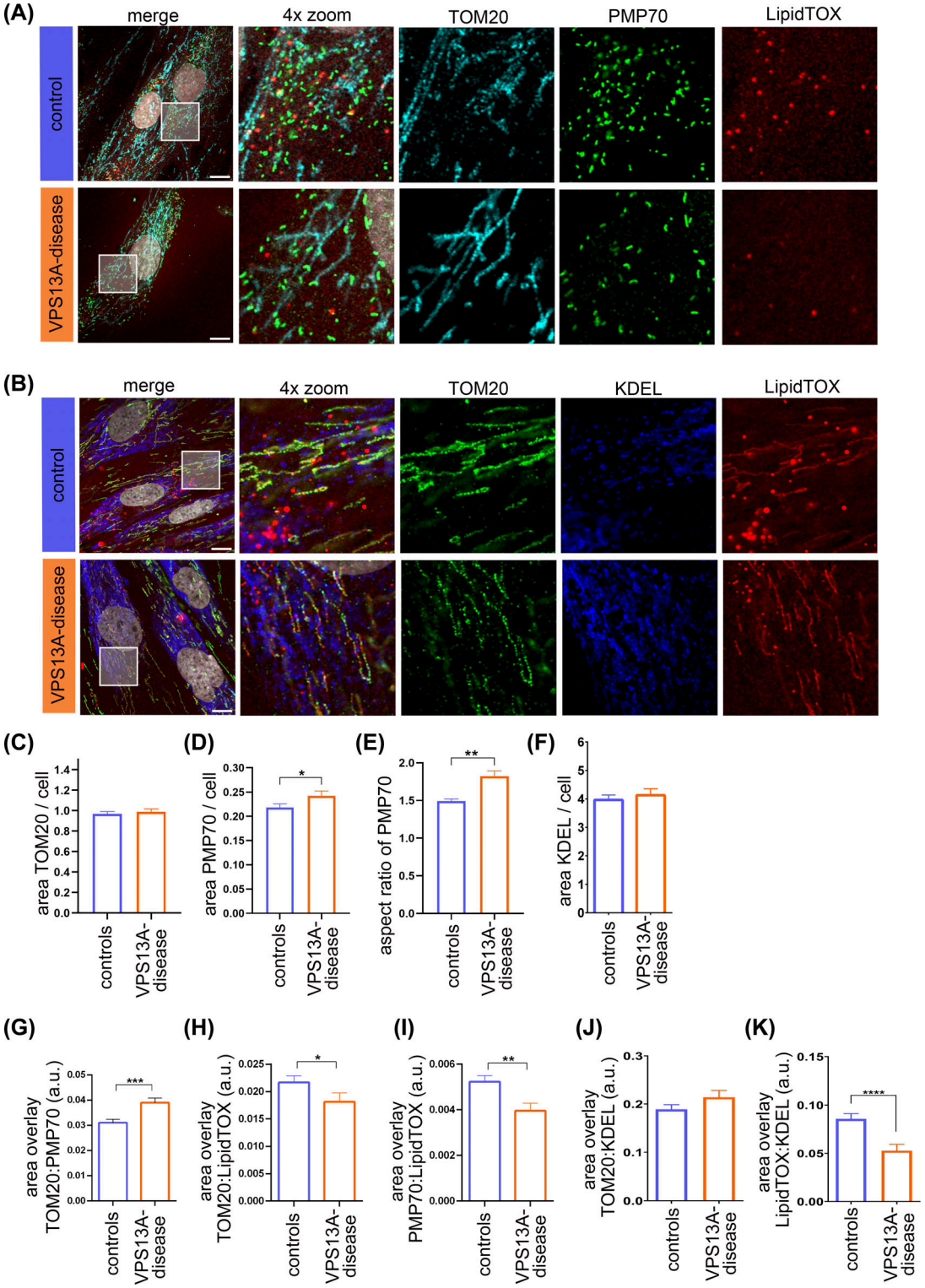

FIG. 2. Alterations of membrane contact sites (MCS) in VPS13A-deficient fibroblasts. (A) Fixed fibroblasts were immunolabeled with an antibody against TOM20 (cyan) and PMP70 (green), then stained with LipidTOX (red) and DAPI (grey). Inlets show areas of 4× magnification. (B) Fixed fibroblasts were immunolabeled with antibodies against TOM20 (green) and KDEL (blue) and stained with LipidTOX (red) and DAPI (grey). Scale bars indicate 10 µm. Quantification of the (C) TOM20 and the (D) PMP70 signal area, normalized per cell (controls: $N = 14$; VPS13A disease: $N = 9$). (E) The aspect ratio of peroxisomes was assessed as the ratio of the minor axis versus the major axis of the PMP70 signal (controls: $N = 14$; VPS13A disease: $N = 9$). (F) Quantification of the KDEL signal area per cell (controls: $N = 9$; VPS13A disease: $N = 6$). Analysis of the overlay area of the signals (G) of TOM20 and PMP70 (controls: $N = 14$; VPS13A disease: $N = 9$), (H) TOM20 and LipidTOX (controls: $N = 14$; VPS13A disease: $N = 9$), (I) PMP70 and LipidTOX (controls: $N = 14$; VPS13A disease: $N = 9$), (J) TOM20 and KDEL (controls: $N = 9$; VPS13A disease: $N = 6$), and (K) KDEL and LipidTOX (controls: $N = 9$; VPS13A disease: $N = 6$); normalized per cell. All data are mean ± standard error of the mean (SEM). Statistical significance calculated by Mann–Whitney test. $^{*}P \leq 0.05$, $^{**}P \leq 0.01$, $^{***}P \leq 0.001$, $^{***}P \leq 0.0001$. [Color figure can be viewed at wileyonlinelibrary.com]

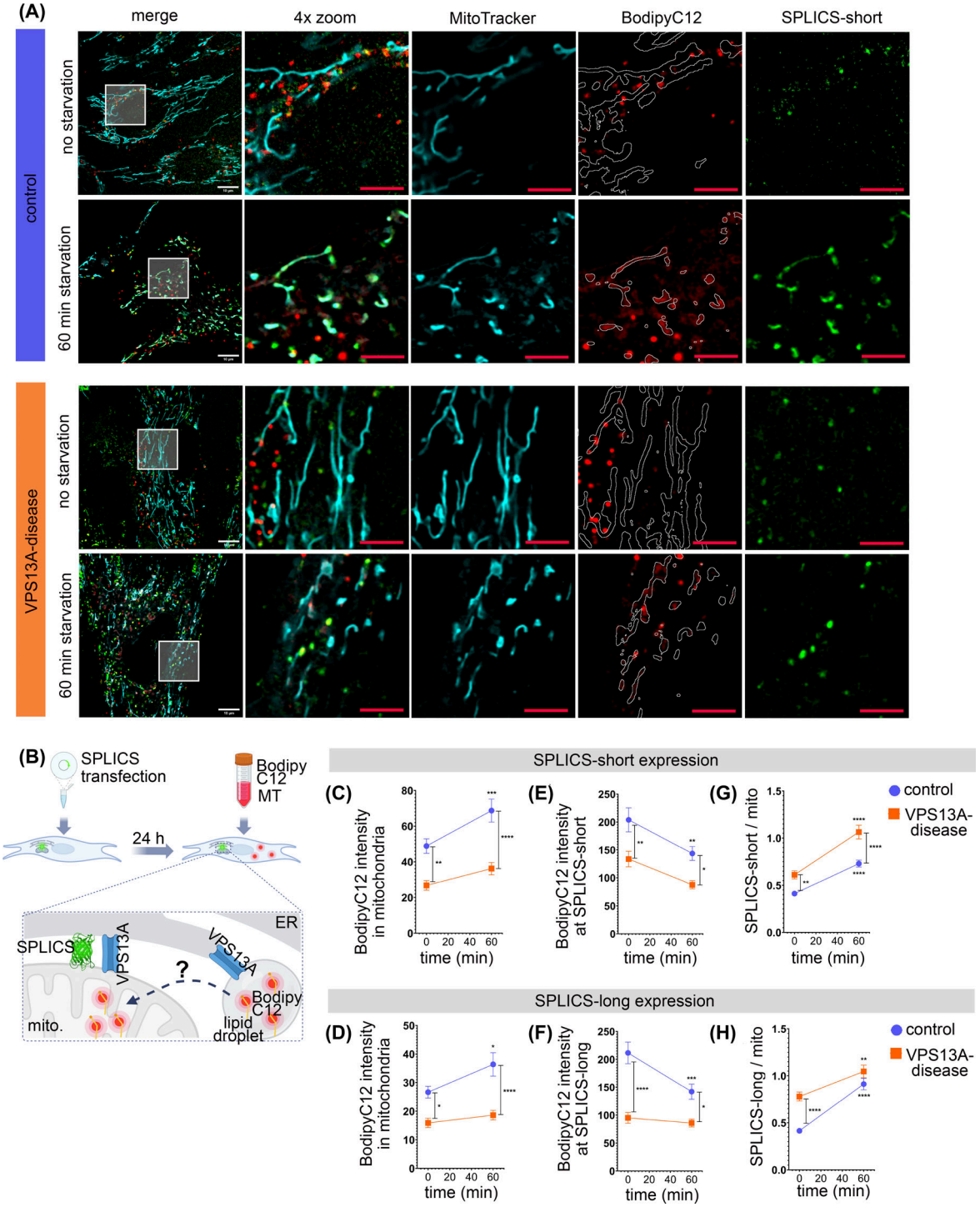

FIG. 3. Impaired fatty acid shuttling in VPS13A-deficient fibroblasts. (A) Fibroblasts were transfected with SPLICS-short or SPLICS-long (green), respectively, and 24 hours post-transfection stained with MitoTracker Deep Red FM (cyan) and BodipyC12 (red). Images were acquired at baseline conditions (0 min), and after 1 hour of starvation. White outlines indicate the outlines of mitochondria within the BodipyC12 image. White scale bar indicates 10 μm, red scale bars indicate 5 μm. (B) Schematic illustration of the experiment setup: fibroblasts expressing SPLICS were stained with BodipyC12 and MitoTracker Deep Red FM (MT). Upon starvation, the BodipyC12 was transferred from the cytosol into the mitochondria. Image generated with Biorender.com. (C),(D) Analysis of mean BodipyC12 intensity inside mitochondria in fibroblasts transfected with (C) SPLICS-short or (D) SPLICS-long. (E),(F) Assessment of the mean BodipyC12 intensity at (E) SPLICS-short or at (F) SPLICS-long. (G),(H) Quantification of the (G) SPLICS-short or (H) SPLICS-long area per mitochondria area. All data are mean ± standard error of the mean (SEM). Statistical significance calculated by two-way analysis of variance (ANOVA) with Sidak's multiple comparison test (controls: $N = 9$; VPS13A disease: $N = 6$) for SPLICS-short and (controls: $N = 6$; VPS13A disease: $N = 4$) for SPLICS-long. $^{*}P \leq 0.05$, $^{**}P \leq 0.01$, $^{***}P \leq 0.001$, $^{****}P \leq 0.0001$. [Color figure can be viewed at wileyonlinelibrary.com]

contact site sensor (SPLICS) for narrow (SPLICS-short) or wide MERCS (SPLICS-long).[23] The transfection efficiencies between fibroblasts and SPLICS-short or SPLICS-long constructs were comparable (Fig. S4G,H). Fibroblasts were subsequently labeled with MitoTracker and the fatty acid BodipyC12 (Fig. 3A). Under starvation, cells switch their metabolism to fatty acid-fueled oxidative phosphorylation, which can be studied by tracing the transfer of BodipyC12 into mitochondria[32] (Fig. 3B). The BodipyC12 intensity inside mitochondria was lower in VPS13A-deficient fibroblasts at baseline. The mitochondrial BodipyC12 intensity increased in controls after 1 hour of starvation, but not in VPS13A-deficient fibroblasts. This was seen in mitochondria expressing SPLICS-short (Figs. 3C and S4A) or SPLICS-long (Figs. 3D and S4B). In controls, the BodipyC12 intensity at SPLICS-short (Figs. 3E and S4C) or SPLICS-long (Figs. 3F and S4D) was significantly higher at baseline, compared with VPS13A-deficient fibroblasts and declined significantly during starvation in controls, but not in VPS13A-deficient fibroblasts. However, over time the BodipyC12 intensity at SPLICS-short (Fig. 3E) or SPLICS-long (Fig. 3F) remained below the BodipyC12 intensity in the controls. Of note, the VPS13A-deficient fibroblasts displayed elevated amounts of SPLICS-short and SPLICS-long at baseline, compared with controls (Figs. 3G,H and S4E,F). Starvation induced an elevation of SPLICS-short (Fig. 3G) or SPLICS-long (Fig. 4H) in both control and VPS13A-deficient fibroblasts. Thin-layer chromatography (TLC) was performed to evaluate to what extent the artificial fatty acid BodipyC12 was metabolized in our cell model. The results show that a small portion is esterified into phospholipids, while the majority remains unchanged within the time frame of the experiment (Fig. S5). Together, these results suggest less effective lipid uptake into mitochondria in VPS13A-deficient fibroblasts under starvation conditions. Additionally, in VPS13A-deficient fibroblasts, the amounts of SPLICS-short and SPLICS-long were elevated.

Phospholipid Shuttling and Autophagosome Formation in VPS13A-Deficient Fibroblasts

For the analysis of phospholipid transfer, mitochondria were loaded with the phospholipid 18:1 NBD-PS (Fig. 4A). Starvation forces phosphatidylserine (PS) shuttling from ER to mitochondria, where it is converted into phosphatidylethanolamine (PE).[33,34] Mitochondria in the VPS13A disease fibroblasts took up significantly less 18:1 NBD-PS. During starvation, the 18:1 NBD-PS signal in mitochondria decreased in control fibroblasts, until it was indistinguishable from VPS13A-deficient fibroblasts after 2 hours (Figs. 4B and S6A).

The shuttling of PS between mitochondria and the ER at MERCS is a prerequisite for autophagosome formation.[35,36] The above-described assay was combined with the autophagosome marker RFP-LC3B (Fig. 4C). The overlapping area of 18:1 NBD-PS with RFP-LC3B was considered an autophagosome (Fig. 4D). Upon starvation, the 18:1 NBD-PS signal inside mitochondria decreased (Figs. 4E and S6B), while at the same time the RFP-LC3B overlapping area with 18:1 NBD-PS signal increased in the control fibroblasts (Figs. 4F and S6C), indicating the formation of autophagosomes. VPS13A-deficient fibroblasts showed significantly more autophagosomes at baseline conditions and no further increase upon starvation (Figs. 4F and S6C). Controls showed a reduction in cytosolic RFP-LC3B upon starvation, while there was no change in the VPS13A-deficient fibroblasts (Figs. 4G and S6D).

As this assay might be prone to artefacts due to the overexpression of RFP-LC3B, we analyzed endogenous levels of LC3B by Western blotting (Fig. 4H). The conversion of cytosolic LC3B-I to membrane-bound LC3B-II is indicative of autophagosome formation. In controls, the ratio of LC3B-II to LC3B-I was slightly increased by starvation and significantly elevated by bafilomycinA1, suggesting efficient autophagosome formation and turnover via autophagy. In VPS13A-deficient fibroblasts we did not observe an increase in the LC3B-II/-I ratio under any treatment condition (Fig. 4I). The quantification of LC3B-I protein revealed no significant changes in any conditions (Fig. 4J), while VPS13A-deficient fibroblasts showed elevated levels of LC3B-II protein compared with control fibroblasts (Fig. 4K).

Together, these findings suggest that autophagy might be impaired in VPS13A-deficient fibroblasts.

Alterations of Mitochondrial Calcium Handling in VPS13A-Deficient Fibroblasts

Previous studies showed diminished store-operated calcium entry (SOCE) in VPS13A-deficient cells.[10,37,38] Since MERCS are crucially involved in calcium transfer between the ER and mitochondria, we analyzed mitochondrial calcium uptake using a protocol previously published by our group.[39] Narrow MERCS, which are involved in this process,[23,39] were visualized by SPLICS-short, mitochondria were stained with MitoTracker, and calcium was assessed by Rhod-2, AM (Fig. 5A). Thapsigargin was used to inhibit the sarcoplasmic/ER calcium ATPase (SERCA), preventing calcium uptake by the ER and forcing mitochondria to buffer calcium.[40] The mitochondrial calcium uptake was blocked by the MCU inhibitor Ru360[41] (Fig. 5B).

In controls, thapsigargin but not the combination of thapsigargin and Ru360 induced a significant elevation in mitochondrial calcium (Figs. 5C and S7A,D,G),

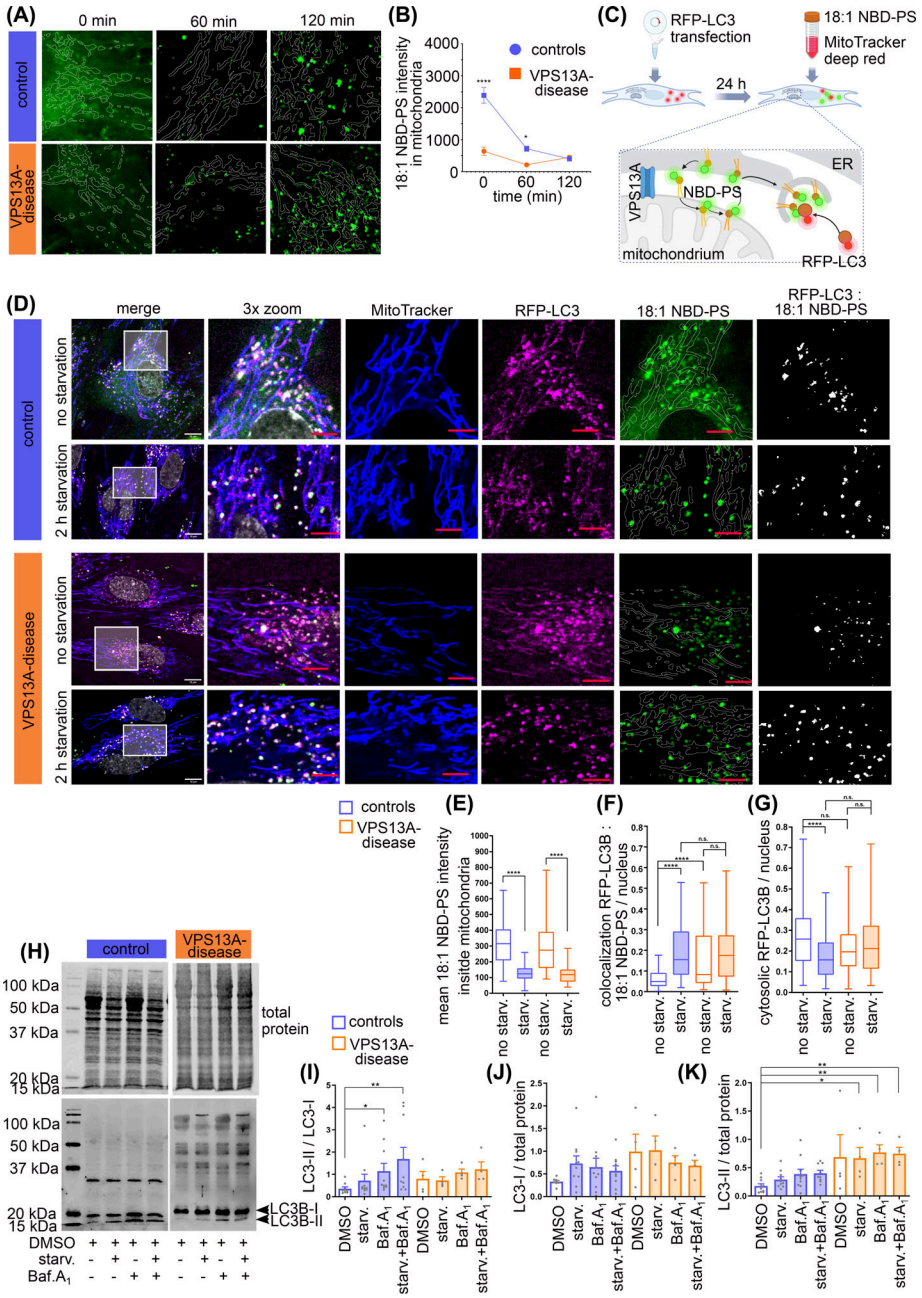

FIG. 4. Impaired phospholipid shuttling in VPS13A-deficient fibroblasts. (A) Fibroblasts were stained with MitoTracker Deep Red FM and loaded with 18:1 NBD-PS (green). White outlines indicate the mitochondria area inside the 18:1 NBD-PS image. (B) Quantification of mean 18:1 NBD-PS signal intensity inside mitochondria (controls: $N = 9$; VPS13A disease: $N = 8$). All data are mean ± standard error of the mean (SEM). Statistical significance calculated by two-way analysis of variance (ANOVA) with Sidak's multiple comparison test. $^{*}P \leq 0.05$, $^{***}P \leq 0.001$. (C) Schematic illustration of the experimental setup: fibroblasts expressing RFP-LC3B were stained with 18:1 NBD-PS and MitoTracker Deep Red FM. 18:1 NBD-PS is integrated into the endoplasmic reticulum (ER) membrane and the mitochondrial membrane. Upon starvation, 18:1 NBD-PS is converted into phosphatidylethanolamine (PE) in the mitochondria and shuttled to the ER at mitochondria–ER contact sites (MERCS). Labeled PE and RFP-LC3B are incorporated into the newly formed autophagosome. Image generated with Biorender.com. (D) Fibroblasts were transfected with RFP-LC3B (magenta) and 24 hours post-transfection loaded with 18:1 NBD-PS (green) and MitoTracker Deep Red FM (blue). White scale bars indicate 10 μm, red scale bars indicate 5 μm. (E) Quantification of the mean 18:1 NBD-PS signal inside the mitochondria. (F) Quantification of colocalization events of the RFP-LC3B and 18:1 NBD-PS, indicating autophagosomes. (G) Quantification of the cytosolic RFP-LC3B signal, outside the mitochondrial as well as outside the 18:1 NBD-PS signal (controls: $N = 9$; VPS13A disease: $N = 7$). All data are median ± minimum/maximum. Statistical significance calculated by Kruskal–Wallis test with Sidak's multiple comparison test. (H) Image of the Western blot for LC3BI/II protein. Fibroblasts were treated with starvation in Hanks' Balanced Salt Solution (HBSS), or with 100 nM bafilomycinA1, or with a combination of starvation in HBSS and 100 nM bafilomycinA1, for 2 hours. (I) Quantification of the ratio of LC3B-II to LC3B-I bands of the Western blot shown in (F). (J) Quantification of LC3B-I bands, normalized to total protein stain shown in (F). (K) Quantification of LC3B-II bands, normalized to total protein stain shown in (F). (controls: $N = 10$; VPS13A disease: $N = 4$). Data are mean ± standard error of the mean (SEM). Statistical significance calculated by Kruskal–Wallis test with Dunn's multiple comparison test. $^{*}P \leq 0.05$, $^{**}P \leq 0.01$, $^{****}P \leq 0.0001$. [Color figure can be viewed at wileyonlinelibrary.com]

while calcium levels remained unchanged at SPLICS-short (Figs. 5D and S7B,E,H). Thapsigargin induced an increase in the amount of SPLICS-short (Figs. 5E and S7C,F,I). In VPS13A fibroblasts, thapsigargin increased mitochondrial calcium, but Ru360 did not prevent mitochondrial calcium uptake (Figs. 5F and S7J,M). Calcium levels remained stable at SPLICS-short (Figs. 5G and S7K,N). The amount of SPLICS-short did not significantly change under any treatment (Figs. 5H and S7L,O). Our findings point to alterations in mitochondrial calcium uptake and insufficient adaptation of narrow MERCS in response to calcium stress in VPS13A-deficient fibroblasts. The MCU is the main channel responsible for mitochondrial calcium influx.[41-43] Western blot analysis showed no differences in MCU expression between control and VPS13A-deficient fibroblasts (Fig. 5I,J).

Discussion

Our systematic evaluation revealed that patient-derived fibroblasts with loss of VPS13A exhibit reduced lipid droplet formation, alterations in various MCS, impaired fatty acid transfer at MERCS, changes in autophagy, and disturbances in mitochondrial calcium uptake.

VPS13A resides at MCS to facilitate the transfer of lipids from one membrane to the other.[12] We found that contact sites between mitochondria and peroxisomes were increased in VPS13A-deficient fibroblasts, whereas contact sites between peroxisomes, the ER, or mitochondria with lipid droplets were decreased. The latter was likely caused by an overall reduction in lipid droplets. Quantification of SPLICS suggests an elevation of MERCS in VPS13A-deficient fibroblasts. There is currently limited literature addressing the phenotypes of MERCS and lipid droplets in cell models with VPS13A deficiency. Our results are in line with the work of Chen and colleagues, showing a reduction in lipid droplets in CRISPR/Cas9 gene edited VPS31A knockout U-2OS cells,[27] while another study in VPS13A knockout MRC5 cells showed reduction in SPLICS-short and SPLICS-long and an increase in lipid droplets.[28] This study identified VPS13A at ER–lipid droplet contact sites to facilitate the lipid transfer required for lipid droplet formation.[28] The contradicting results highlight the need for more research to investigate the underlying mechanisms. Alterations in lipid droplets have been implicated also in other neurodegenerative diseases such as Parkinson's,[44,45] Huntington's[46,47] or Alzheimer's disease.[48] One possibility is that MERCS and lipid droplets are regulated differently in different tissues, depending on the specific requirements of different cell types. Lipid droplets are dynamic organelles, which are fueled with lipids from the ER[49] and serve as storage organelles to provide fatty acids for β-oxidation to mitochondria under conditions of high energy demand.[50,51] Furthermore, it should be emphasized that unlike other studies with an isogenic background, our study was the first to use fibroblasts from unrelated control subjects and VPS13A disease patients with the persons' individual genetic background, which could conceivably contribute to VPS13A-related pathology. However, this contributes to the high variability in some experiments, which, together with the small number of fibroblast lines, is a limitation of our study and calls for further validation work in the future.

It is currently assumed that VPS13A transfers phospholipids between membranes.[12,52] We hypothesized that loss of VPS13A may lead to a general disruption of lipid metabolism, and we investigated fatty acid transfer in mitochondria under metabolic stress. Our results indicate a reduction in fatty acid transfer into mitochondria. Yet, this does not indicate that VPS13A directly transfers fatty acids. However, it is noteworthy that for VPS13D, which is structurally and functionally closely related to VPS13A,[53] a function in fatty acid transfer between lipid droplets and mitochondria has been described.[54] Our results could, however, be indirectly associated with loss of VPS13A in that the impaired fatty acid uptake could be a sign of a general disturbance of lipid distribution and/or metabolism.

We furthermore showed alterations in autophagy in VPS13A-deficient fibroblasts. Previous studies described impaired autophagic flux in *VPS13A*-knockdown HeLa cells[55] and during erythroid maturation of patients with VPS13A disease.[8] Impaired autophagy might arise from an endo-/lysosomal dysfunction, thereby inhibiting autophagic turnover.[56] VPS13A interacts with the lipid scramblase ATG9A to facilitate phospholipid transfer at MERCS for autophagosome formation.[57] Of note, the formation of autophagosomes is a redundant process and also functions via the lipid transfer protein ATG2 interacting with ATG9A,[57] consistent with our observations that autophagosome formation is nonetheless functional in VPS13A-deficient cells. VPS13A and ATG2 belong to the same family of lipid transfer proteins.[35,52,57-59]

Additionally, we investigated the influence of VPS13A deficiency on calcium homeostasis. Diminished SOCE, the influx of calcium across the plasma membrane into the cell, was observed in VPS13A-deficient fibroblasts and induced pluripotent stem cell (iPSC)-derived neurons.[10,37,38] However, data on mitochondrial calcium homeostasis are lacking. Narrow MERCS appear to be primarily responsible for calcium flux into mitochondria,[23,39] and since we have already seen an altered response in narrow MERCS to metabolic stress, we wanted to find out whether the loss of VPS13A also has an effect on narrow MERCS-mediated mitochondrial calcium homeostasis. Consistent with our previous study,[39] healthy cells appropriately increase

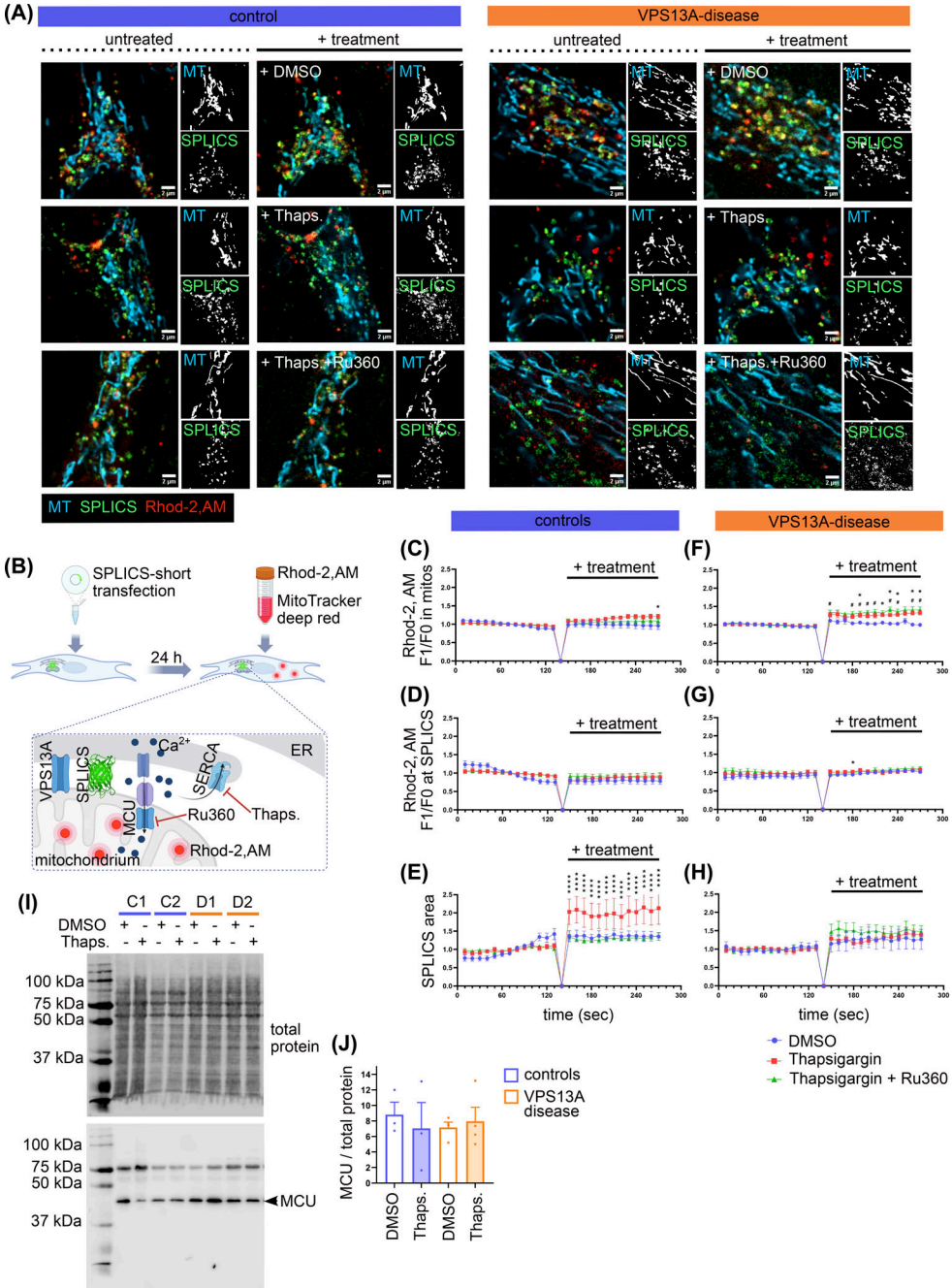

FIG. 5. Impaired mitochondrial calcium handling in VPS13A-deficient fibroblasts. (A) Fibroblasts were transfected with SPLICS-short (green) and 24 hours later stained with MitoTracker Deep Red FM (cyan) and Rhod-2, AM (red). Images were acquired for 2 minutes at 10-second intervals at baseline conditions (left image panels) and for 2 minutes at 10-seccond intervals after treatment application (dimethyl sulfoxide [DMSO], 1 μM thapsigargin or 1 μM thaspigargin +10 μM Ru360; right image panels). Scale bars indicate 2 μm. (B) Schematic illustration of the experimental setup: fibroblasts expressing SPLICS-short were stained with Rhod-2, AM and MitoTracker Deep Red FM. Calcium is shuttled from the endoplasmic reticulum (ER) and the cytosol into the mitochondria at mitochondria–ER contact sites (MERCS), via voltage-dependent anion channel (VDAC) and mitochondrial calcium uniporter (MCU) calcium channels. Rhod-2, AM intensity indicates mitochondrial calcium levels, MitoTracker Deep Red FM was used to identify mitochondria. Thapsigargin is an inhibitor of sarcoplasmic/ER calcium ATPase (SERCA), blocking calcium uptake into the ER, resulting in elevation in cytosolic calcium levels. Ru360 inhibits the MCU, preventing mitochondrial calcium uptake. (C) Mean Rhod-2, AM intensity inside mitochondria in control fibroblasts. (D) Mean Rhod-2, AM intensity at SPLICS-short in control fibroblasts. (E) Quantification of SPLICS-short area in control fibroblasts. (F) Mean Rhod-2, AM intensity inside mitochondria in VPS13A-deficient fibroblasts. (G) Mean Rhod-2, AM intensity at SPLICS-short in VPS13A-deficient fibroblasts. (H) Quantification of SPLICS-short area in VPS13A-deficient fibroblasts (controls: $N = 11$; VPS13A disease: $N = 6$). All data are mean ± standard error of the mean (SEM). Statistical significance calculated by two-way analysis of variance (ANOVA) with Dunnett's multiple comparison test. $^{*}P \leq 0.05$, $^{**}P \leq 0.01$, $^{****}P \leq 0.0001$. (I) Fibroblasts were treated with DMSO or 1 μM thapsigargin for 1 hour and subsequently lyzed for Western blot analysis of MCU protein level. Total protein stain served as loading control. (J) Quantification of the MCU protein bands, normalized to total protein staining. All data are mean ± SEM (controls: $N = 3$; VPS13A disease: $N = 4$). Statistical significance calculated by two-way ANOVA with Dunnett's multiple comparison test. [Color figure can be viewed at wileyonlinelibrary.com]

mitochondrial calcium levels upon thapsigargin treatment, along with a dynamic reorganization of narrow MERCS. Surprisingly, however, mitochondria in VPS13A disease fibroblasts accumulated calcium also under conditions of MCU inhibition. The MCU is the main channel for mitochondrial calcium uptake.[41-43] Changes in the composition of the protein complex of MCU, MICU1, and EMRE can lead to alterations in the sensitivity of MCU against Ru360.[60-62] We did not observe alterations in MCU protein levels in VPS13A-deficient fibroblasts. The inability to structurally reorganize the initially elevated SPLICS-labeled narrow MERCS under calcium stress is remarkably similar to a previously described phenotype in Parkinson's models with deficiency in the MERCS regulating proteins Parkin or PINK1.[39]

Taken together, our data suggest that VPS13A-deficiency leads to disturbances of MCS beyond impaired lipid transfer, including changes in mitochondrial calcium handling, in that the mitochondria still take up calcium though the cells were exposed to the MCU inhibitor Ru360. However, further studies are required to determine the extent to which this alteration of calcium handling affects mitochondrial function and maintenance and is related to the previously described changes in SOCE. Also, the link between impaired lipid and calcium transfer at MERCS in VPS13A-deficient cells warrants further investigation.

Author Roles: (1) Research Project: A. Conception, B. Design, C. Execution, D. Data Analysis; (2) Statistical Analysis: A. Design, B. Execution, C. Review and Critique; (3) Manuscript Preparation: A. Writing of the First Draft, B. Editing of the Final Version.
D.G.: 1A, 1B, 1C, 1D, 2A, 2B, 3A, 3B.
A.S.: 1C, 1D, 3B.
E.F.: 1C, 1D, 3B.
J.W.S.: 1C, 3B.
J.L.: 1C, 1D, 3B.
H.G.: 1D, 3B.
S.K.: 1C.
M.U.D.T.: 1C.
A.E.B.: 1C, 3B.
A.H.: 1A, 1B, 2C, 3B.
K.P.: 1A, 1B, 3A, 3B.

Acknowledgments: The super-resolution imaging was performed using an LSM900 Airyscan microscope (Zeiss; DFG §91, INST 264/175-1 FUGG). Thanks to Dr. Daniela Volke and Prof. Dr. Ralf Hoffmann (Center for Biotechnology and Biomedicine, Leipzig) for sharing the FLA5000 digital visualizer (FUJIFILM, Düsseldorf, Germany) which was used for the Bodipy C12 detection on thin-layer chromatography plates. Open Access funding enabled and organized by Projekt DEAL.

Financial Disclosures (for the Preceding 12 Months): A.H. has received funding from the European Social Fonds, the Federal Ministry of Education and Research, and the Hermann und Lilly Schilling-Stiftung für medizinische Forschung im Stifterverband. He has received royalties from Elsevier Press and Kohlhammer. K.P. was supported by Rostock Academy of Science (RAS).

Data Availability Statement

The data that support the findings of this study are available from the corresponding author upon reasonable request.

References

1. Peikert K, Dobson-Stone C, Rampoldi L, et al. *VPS13A* Disease. In: GeneReviews® [Internet], Adam MP, Feldman J, Mirzaa GM, et al, editors. Seattle, WA: University of Washington; 1993.
2. Walker RH, Peikert K, Jung HH, Hermann A, Danek A. Neuroacanthocytosis syndromes: the clinical perspective. Contact (Thousand Oaks) 2023;6:625152564231210339. https://doi.org/10.1177/25152564231210339
3. Walterfang M, Evans A, Looi JCL, et al. The neuropsychiatry of neuroacanthocytosis syndromes. Neurosci Biobehav Rev 2011;35(5):1275–1283. https://doi.org/10.1016/j.neubiorev.2011.01.001
4. Ditzel RM, Walker RH, Nirenberg MJ, et al. An autopsy series of seven cases of VPS13A disease (chorea-acanthocytosis). Mov Disord 2023;38(12):2163–2172. https://doi.org/10.1002/mds.29589
5. Föller M, Hermann A, Gu S, et al. Chorein-sensitive polymerization of cortical actin and suicidal cell death in chorea-acanthocytosis. FASEB J 2012;26(4):1526–1534. https://doi.org/10.1096/fj.11-198317
6. Glaß H, Neumann P, Pal A, et al. Combined dendritic and axonal deterioration are responsible for motoneuronopathy in patient-derived neuronal cell models of chorea-acanthocytosis. Int J Mol Sci 2020;21(5):1797. https://doi.org/10.3390/ijms21051797
7. Glaß H, Pal A, Reinhardt P, et al. Defective mitochondrial and lysosomal trafficking in chorea-acanthocytosis is independent of Src-kinase signaling. Mol Cell Neurosci 2018;92:137–148. https://doi.org/10.1016/j.mcn.2018.08.002
8. Lupo F, Tibaldi E, Matte A, et al. A new molecular link between defective autophagy and erythroid abnormalities in chorea-acanthocytosis. Blood 2016;128(25):2976–2987. https://doi.org/10.1182/blood-2016-07-727321
9. Peikert K, Federti E, Matte A, et al. Therapeutic targeting of Lyn kinase to treat chorea-acanthocytosis. Acta Neuropathol Commun 2021;9(1):81. https://doi.org/10.1186/s40478-021-01181-y
10. Pelzl L, Hauser S, Elsir B, et al. Lithium sensitive ORAI1 expression, store operated Ca2+ entry and suicidal death of neurons in chorea-acanthocytosis. Sci Rep 2017;7(1):6457. https://doi.org/10.1038/s41598-017-06451-1
11. Braschi B, Bruford EA, Cavanagh AT, Neuman SD, Bashirullah A. The bridge-like lipid transfer protein (BLTP) gene group: introducing new nomenclature based on structural homology indicating shared function. Hum Genomics 2022;16(1):66. https://doi.org/10.1186/s40246-022-00439-3
12. Hanna M, Guillén-Samander A, de Camilli P. RBG motif bridge-like lipid transport proteins: structure, functions, and open questions. Annu Rev Cell Dev Biol 2023;39:409–434. https://doi.org/10.1146/annurev-cellbio-120420-014634
13. Guillén-Samander A, Wu Y, Pineda SS, et al. A partnership between the lipid scramblase XK and the lipid transfer protein VPS13A at the plasma membrane. Proc Natl Acad Sci U S A 2022;119(35):e2205425119. https://doi.org/10.1073/pnas.2205425119
14. Kumar N, Leonzino M, Hancock-Cerutti W, et al. VPS13A and VPS13C are lipid transport proteins differentially localized at ER contact sites. J Cell Biol 2018;217(10):3625–3639. https://doi.org/10.1083/jcb.201807019
15. Park J-S, Hu Y, Hollingsworth NM, Miltenberger-Miltenyi G, Neiman AM. Interaction between VPS13A and the XK scramblase is important for VPS13A function in humans. J Cell Sci 2022;135(17):jcs260227. https://doi.org/10.1242/jcs.260227
16. Helle SCJ, Kanfer G, Kolar K, Lang A, Michel AH, Kornmann B. Organization and function of membrane contact sites. Biochim Biophys Acta 2013;1833(11):2526–2541. https://doi.org/10.1016/j.bbamcr.2013.01.028
17. Lee S, Min K-T. The interface between ER and mitochondria: molecular compositions and functions. Mol Cells 2018;41(12):1000–1007. https://doi.org/10.14348/molcells.2018.0438
18. Petrungaro C, Kornmann B. Lipid exchange at ER-mitochondria contact sites: a puzzle falling into place with quite a few pieces missing. Curr Opin Cell Biol 2019;57:71–76. https://doi.org/10.1016/j.ceb.2018.11.005

19. Moltedo O, Remondelli P, Amodio G. The mitochondria-endoplasmic reticulum contacts and their critical role in aging and age-associated diseases. Front Cell Dev Biol 2019;7:172. https://doi.org/10.3389/fcell.2019.00172

20. Sammeta SS, Banarase TA, Rahangdale SR, et al. Molecular understanding of ER-MT communication dysfunction during neurodegeneration. Mitochondrion 2023;72:59–71. https://doi.org/10.1016/j.mito.2023.07.005

21. Sathyamurthy VH, Nagarajan Y, Parvathi VD. Mitochondria-endoplasmic reticulum contact sites (MERCS): a new axis in neuronal degeneration and regeneration. Mol Neurobiol 2024;61(9):6528–6538. https://doi.org/10.1007/s12035-024-03971-6

22. McLelland G-L, Goiran T, Yi W, et al. Mfn2 ubiquitination by PINK1/parkin gates the p97-dependent release of ER from mitochondria to drive mitophagy. Elife 2018;7:7. https://doi.org/10.7554/eLife.32866

23. Cieri D, Vicario M, Giacomello M, et al. SPLICS: a split green fluorescent protein-based contact site sensor for narrow and wide heterotypic organelle juxtaposition. Cell Death Differ 2018;25(6):1131–1145. https://doi.org/10.1038/s41418-017-0033-z

24. Hamasaki M, Furuta N, Matsuda A, et al. Autophagosomes form at ER-mitochondria contact sites. Nature 2013;495(7441):389–393. https://doi.org/10.1038/nature11910

25. Giacomello M, Pellegrini L. The coming of age of the mitochondria-ER contact: a matter of thickness. Cell Death Differ 2016;23(9):1417–1427. https://doi.org/10.1038/cdd.2016.52

26. Schindelin J, Arganda-Carreras I, Frise E, et al. Fiji: an open-source platform for biological-image analysis. Nat Methods 2012;9(7):676–682. https://doi.org/10.1038/nmeth.2019

27. Chen S, Roberts MA, Chen CY, et al. VPS13A and VPS13C influence lipid droplet abundance. Contact (Thousand Oaks) 2022;5:25152564221125613. https://doi.org/10.1177/25152564221125613

28. Yeshaw WM, van der Zwaag M, Pinto F, et al. Human VPS13A is associated with multiple organelles and influences mitochondrial morphology and lipid droplet motility. Elife 2019;8:8. https://doi.org/10.7554/eLife.43561

29. Kleiboeker B, Lodhi IJ. Peroxisomal regulation of energy homeostasis: effect on obesity and related metabolic disorders. Mol Metab 2022;65:101577. https://doi.org/10.1016/j.molmet.2022.101577

30. Mast FD, Fagarasanu A, Knoblach B, Rachubinski RA. Peroxisome biogenesis: something old, something new, something borrowed. Physiology (Bethesda) 2010;25(6):347–356. https://doi.org/10.1152/physiol.00025.2010

31. Jacquemyn J, Cascalho A, Goodchild RE. The ins and outs of endoplasmic reticulum-controlled lipid biosynthesis. EMBO Rep 2017;18(11):1905–1921. https://doi.org/10.15252/embr.201643426

32. Rambold AS, Cohen S, Lippincott-Schwartz J. Fatty acid trafficking in starved cells: regulation by lipid droplet lipolysis, autophagy, and mitochondrial fusion dynamics. Dev Cell 2015;32(6):678–692. https://doi.org/10.1016/j.devcel.2015.01.029

33. Gomez-Suaga P, Paillusson S, Stoica R, Noble W, Hanger DP, Miller CCJ. The ER-mitochondria tethering complex VAPB-PTPIP51 regulates autophagy. Curr Biol 2017;27(3):371–385. https://doi.org/10.1016/j.cub.2016.12.038

34. Ktistakis NT. ER platforms mediating autophagosome generation. Biochim Biophys Acta Mol Cell Biol Lipids 2020;1865(1):158433. https://doi.org/10.1016/j.bbalip.2019.03.005

35. Dabrowski R, Tulli S, Graef M. Parallel phospholipid transfer by Vps13 and Atg2 determines autophagosome biogenesis dynamics. J Cell Biol 2023;222(7):e202211039. https://doi.org/10.1083/jcb.202211039

36. Isola D, Elazar Z. Phospholipid supply for autophagosome biogenesis. J Mol Biol 2024;436(15):168691. https://doi.org/10.1016/j.jmb.2024.168691

37. Pelzl L, Elsir B, Sahu I, et al. Lithium sensitivity of store operated Ca2+ entry and survival of fibroblasts isolated from chorea-acanthocytosis patients. Cell Physiol Biochem 2017;42(5):2066–2077. https://doi.org/10.1159/000479901

38. Sukkar B, Hauser S, Pelzl L, et al. Inhibition of lithium sensitive Orai1/ STIM1 expression and store operated Ca2+ entry in chorea-Acanthocytosis neurons by NF-κB inhibitor Wogonin. Cell Physiol Biochem 2018;51(1):278–289. https://doi.org/10.1159/000495229

39. Grossmann D, Malburg N, Glaß H, et al. Mitochondria-endoplasmic-reticulum contact sites dynamics and calcium homeostasis are differentially disrupted in PINK1-PD or PRKN-PD neurons. Mov Disord 2023;38(10):1822–1836. https://doi.org/10.1002/mds.29525

40. Lytton J, Westlin M, Hanley MR. Thapsigargin inhibits the sarcoplasmic or endoplasmic reticulum Ca-ATPase family of calcium pumps. J Biol Chem 1991;266(26):17067–17071.

41. Kirichok Y, Krapivinsky G, Clapham DE. The mitochondrial calcium uniporter is a highly selective ion channel. Nature 2004;427(6972):360–364. https://doi.org/10.1038/nature02246

42. Baughman JM, Perocchi F, Girgis HS, et al. Integrative genomics identifies MCU as an essential component of the mitochondrial calcium uniporter. Nature 2011;476(7360):341–345. https://doi.org/10.1038/nature10234

43. Drago I, Pizzo P, Pozzan T. After half a century mitochondrial calcium in- and efflux machineries reveal themselves. EMBO J 2011;30(20):4119–4125. https://doi.org/10.1038/emboj.2011.337

44. Boutant M, Kulkarni SS, Joffraud M, et al. Mfn2 is critical for brown adipose tissue thermogenic function. EMBO J 2017;36(11):1543–1558. https://doi.org/10.15252/embj.201694914

45. Halliday GM, Ophof A, Broe M, et al. Alpha-synuclein redistributes to neuromelanin lipid in the substantia nigra early in Parkinson's disease. Brain 2005;128(Pt 11):2654–2664. https://doi.org/10.1093/brain/awh584

46. Aditi K, Shakarad MN, Agrawal N. Altered lipid metabolism in drosophila model of Huntington's disease. Sci Rep 2016;6:31411. https://doi.org/10.1038/srep31411

47. Martinez-Vicente M, Talloczy Z, Wong E, et al. Cargo recognition failure is responsible for inefficient autophagy in Huntington's disease. Nat Neurosci 2010;13(5):567–576. https://doi.org/10.1038/nn.2528

48. Puglielli L, Tanzi RE, Kovacs DM. Alzheimer's disease: the cholesterol connection. Nat Neurosci 2003;6(4):345–351. https://doi.org/10.1038/nn0403-345

49. Na H, Zhang P, Ding Y, et al. Proteomic studies of isolated lipid droplets from bacteria, C. elegans, and mammals. Methods Cell Biol 2013;116:1–14. https://doi.org/10.1016/B978-0-12-408051-5.00001-2

50. Reue K. A thematic review series: lipid droplet storage and metabolism: from yeast to man. J Lipid Res 2011;52(11):1865–1868. https://doi.org/10.1194/jlr.E020602

51. Schuldiner M, Bohnert M. A different kind of love - lipid droplet contact sites. Biochim Biophys Acta Mol Cell Biol Lipids 2017;1862(10 Pt B):1188–1196. https://doi.org/10.1016/j.bbalip.2017.06.005

52. Reinisch KM, de Camilli P, Melia TJ. Lipid dynamics at membrane contact sites. Annu Rev Biochem 2025;94(1):479–502. https://doi.org/10.1146/annurev-biochem-083024-122821

53. Dziurdzik SK, Conibear E. The Vps13 family of lipid transporters and its role at membrane contact sites. Int J Mol Sci 2021;22(6):2905. https://doi.org/10.3390/ijms22062905

54. Wang J, Fang N, Xiong J, Du Y, Cao Y, Ji W-K. An ESCRT-dependent step in fatty acid transfer from lipid droplets to mitochondria through VPS13D-TSG101 interactions. Nat Commun 2021;12(1):1252. https://doi.org/10.1038/s41467-021-21525-5

55. Muñoz-Braceras S, Calvo R, Escalante R. TipC and the chorea-acanthocytosis protein VPS13A regulate autophagy in Dictyostelium and human HeLa cells. Autophagy 2015;11(6):918–927. https://doi.org/10.1080/15548627.2015.1034413

56. Muñoz-Braceras S, Tornero-Écija AR, Vincent O, Escalante R. VPS13A is closely associated with mitochondria and is required for efficient lysosomal degradation. Dis Model Mech 2019;12(2). https://doi.org/10.1242/dmm.036681

57. van Vliet AR, Jefferies HBJ, Faull PA, et al. Exploring the ATG9A interactome uncovers interaction with VPS13A. J Cell Sci 2024;137(4):jcs261081. https://doi.org/10.1242/jcs.261081

58. Leonzino M, Reinisch KM, De Camilli P. Insights into VPS13 properties and function reveal a new mechanism of eukaryotic lipid

transport. Biochim Biophys Acta Mol Cell Biol Lipids 2021; 1866(10):159003. https://doi.org/10.1016/j.bbalip.2021.159003

59. Ugur B, Hancock-Cerutti W, Leonzino M, De Camilli P. Role of VPS13, a protein with similarity to ATG2, in physiology and disease. Curr Opin Genet Dev 2020;65:61–68. https://doi.org/10.1016/j.gde.2020.05.027
60. Paillard M, Csordás G, Huang K-T, Várnai P, Joseph SK, Hajnóczky G. MICU1 interacts with the D-ring of the MCU pore to control its Ca2+ flux and sensitivity to Ru360. Mol Cell 2018; 72(4):778–785.e3. https://doi.org/10.1016/j.molcel.2018.09.008
61. Patron M, Sprenger H-G, Langer T. M-AAA proteases, mitochondrial calcium homeostasis and neurodegeneration. Cell Res 2018; 28(3):296–306. https://doi.org/10.1038/cr.2018.17
62. Rodríguez-Prados M, Huang KT, Márta K, et al. MICU1 controls the sensitivity of the mitochondrial Ca2+ uniporter to activators and inhibitors. Cell Chem Biol 2023;30(6):606–617.e4. https://doi.org/10.1016/j.chembiol.2023.05.002
63. Folch J, Lees M, Sloane Stanley GH. A simple method for the isolation and purification of total lipides from animal tissues. J Biol Chem 1957;226(1):497–509.
64. Fuchs B, Schiller J, Süss R, Schürenberg M, Suckau D. A direct and simple method of coupling matrix-assisted laser desorption and ionization time-of-flight mass spectrometry (MALDI-TOF MS) to thin-layer chromatography (TLC) for the analysis of phospholipids from egg yolk. Anal Bioanal Chem 2007;389(3):827–834. https://doi.org/10.1007/s00216-007-1488-4

Supporting Data

Additional Supporting Information may be found in the online version of this article at the publisher's web-site.